Electronic Supplementary Material (ESI) for ChemComm.

Eshelby Untwisting

Xiaodi Zhong, Hengyu Zhou, Chao Li, Alexander G. Shtukenberg, Michael D. Ward,* Bart Kahr*

Department of Chemistry and the Molecular Design Institute, New York University, New York City, New York 10003, United States

Supplementary Information

Table of contents

Crystallography. Crystallographic information files (CIF) for benzil were retrieved from the Cambridge Structural Database.

- $P3_121$ space group: CSD REFCODE BENZIL05; Deposition Number 1108768; M. More, G. Odou and J. Lefebvre, *Acta Crystallogr. Sect. B: Struct. Sci*., 1987, **43**, 398.
- $P3_221$ space group: CSD REFCODE BENZIL06; Deposition Number 1859205; V. P. Charpe, A. Sagadevan and K. C. Hwang, *Green Chem.*, 2020, **22**, 4426, DOI: 10.1039/D0GC00975J.

Simulation parameters. Partial charges, atomic masses, lattice parameters and force field parameters are the same with a previous report from are laboratory describing twisting crystals *in silico* (see: C. Li, A. G. Shtukenberg, E. Efrati, L. Vogt-Maranto, P. Raiteri, J. D. Gale, A. L. Rohl and B. Kahr, *J. Phys. Chem. C*. 2020, **124**, 15616–15624). Partial charges and atomic masses used here are contained in the tables below. Crystal lattice parameters for benzil were obtained from the CSD structures above.

Table S1. Partial atomic charges and masses for benzil

	Atom type	Charge	Mass (amu)
C1	C	0.4095	12.010
C2	CA	-0.0427	12.010
C3	CA	-0.1065	12.010
C4	CA	-0.1378	12.010
C5	CA	-0.1040	12.010
C6	CA	-0.1378	12.010
C7	CA	-0.1065	12.010
O1	O	-0.4459	16.000
H1	H	0.1337	1.008
H2	H	0.1342	1.008
H3	H	0.1359	1.008
H4	H	0.1342	1.008
H5	H	0.1337	1.008
C1C	C	0.4095	12.010
C2C	CA	-0.0427	12.010
O1C	O	-0.4459	16.000
C3C	CA	-0.1065	12.010
C7C	CA	-0.1065	12.010
C4C	CA	-0.1378	12.010
H1C	H	0.1337	1.008
C6C	CA	-0.1378	12.010
H5C	H	0.1337	1.008
C5C	CA	-0.1040	12.010
H2C	H	0.1342	1.008
H4C	H	0.1342	1.008

H3C	H	0.1359	1.008

Table S2. Force field parameters

S.2.1. Covalent Bond Parameters

I-J	k_r	r_{eq}
CA-CA	20.7455	1.3870
C-CA	15.1645	1.4870
C-O	28.1001	1.2140
C-C	12.5800	1.5500
CA-H	14.9304	1.0870

S.2.2. Covalent Angle Parameters

I-J-K	k_θ	θ_{eq}
CA-CA-CA	2.9132	119.9701
C-CA-CA	2.8031	120.1401
CA-C-O	2.9778	123.4401
C-C-CA	2.6769	118.3401
C-C-O	2.9124	120.9901
CA-CA-H	2.1014	120.0101

S.2.3. Covalent Dihedral Parameters

I-J-K-L	k_1	k_2	k_3
CA-CA-CA-CA	0	0.1572	0
C-CA-CA-CA	0	0.1572	0
CA-CA-C-O	0	0.0434	0
C-C-CA-CA	0	0.0434	0
CA-C-C-O	0	0.0130	0
CA-C-C-CA	0	0.0130	0
O-C-C-O	0	0.0130	0
CA-CA-CA-H	0	0.1572	0
H-CA-CA-H	0	0.1572	0
C-CA-CA-H	0	0.1572	0

S.2.4. Covalent Improper Dihedral Parameters

I-J-K-L	k	d	n
CA-C-CA-CA	0.0477	-1	2
C-C-CA-O	0.4553	-1	2
CA-CA-CA-H	0.0477	-1	2

S.2.5. Pair Potentials

I/J	ε	σ
CA	0.0037	3.3997
H	0.0007	2.5996
C	0.0037	3.3997
O	0.0091	2.9599

Simulation details

Hexagonal rods of benzil (space groups $P3_121$ and $P3_221$) for simulations were constructed from the CIF files by Python codes, with lattice parameters determined at 100 K fixed at $a = b = 8.356(3)$ Å and $c = 13.375(6)$ Å. The sizes of the rods were 15 unit cells along the c axis, and 4, 6, 8, or 10 unit cells along a. Each unit cell was assigned a unique set of coordinates, and screw dislocations of Burgers vector **b** = <000±1> were generated by moving the coordinates of the unit cells on a chosen shear plane from 0 to **b**. This dislocation core associated with this displacement extended evenly over 3 unit cells on that shear direction for all rods, regardless of rod size. For a right-handed screw dislocation, molecules outside the dislocation core were raised uniformly along [0001] from zero to **b** when rotating by 2π around the core, producing shears in the $(2\bar{1}\bar{1}0)$ or $(1\ 0\bar{1}0)$ planes. The magnitude of the displacement, z, of the molecules along c was calculated as:

$$z = \frac{b}{2\pi} tan^{-1} \frac{y}{x}.$$

Geometry optimizations and MD simulations using the Generalized Amber Force Field (GAFF)[1,2] were conducted with the Large-scale Atomic/Molecular Massively Parallel Simulator (LAMMPS) code.[3] The benzil nanorods were located in the centre of a simulation box, and the distances between the crystal surfaces and the box boundaries were > 15 Å in orthogonal directions. Partial atomic charges were derived from a restrained electrostatic potential (RESP) calculation with the HF/6-31G* basis set using the R.E.D. web server.[4,5,6,7] The General Utility Lattice Program (GULP) was used to calculate the improper four-body interaction torsional potentials with the introduction of equilibrium values in the angular dependencies torsional angle.[8,9] Mechanical distortions were in the non-activated, energy barrier-free processes. Energy minimisation was achieved by conjugate gradient minimization with a relative energy tolerance of 10^{-8}. Relaxation was sped by iterative cycles of geometry optimization, followed by Molecular Dynamics (MD) performed at 200 K with the NVE microcanonical ensemble controlled by a Langevin thermostat

with a timestep of 1 fs. The cut-off distance for pairwise Lennard Jones interactions was set to 12.5 Å, while the electrostatic interactions beyond 12.5 Å were calculated in reciprocal space using the particle-particle particle-mesh *k*-space method. Trajectories were recorded every 500 fs for periods of 5 ns until the twisting angle was unchanging within <2% over a period of 0.2 ns. Twisting angle calculations, potential energy visualizations and torsion angle statistics were completed using Python codes.

The LAMMPS input file and Python codes for creating crystals from CIF, calculating twisting angles, potential energy visualization, and torsion angle analysis can be found on https://github.com/hz2134-chem/KahrWardGroup.

Calculation of the twist angles

Benzil molecules on the corners and edges of the crystals are more poorly coordinated. Calculation of twisting angles were based on molecules inside the crystal. Molecules on the surface were excluded. Unit cells within layers positioned at ¼ and ¾ along *c* of the crystal were selected. For example, as ~~in~~ in Figure S1~~Figure S1~~, the 4th layer and the 12th layer were selected, in a crystal with a height of 15 unit cells. In these two layers, the vectors (such as v_1 and v_2) connecting the third unit cells from the outermost surface (unit cells highlighted in Figure S1~~Figure S1~~), along six directions of the hexagonal cross section, were used for calculation of twisting angles in each frame. These angles were averaged over 0.1 ns, at the last stages of simulation when twisting angles were stabilized.

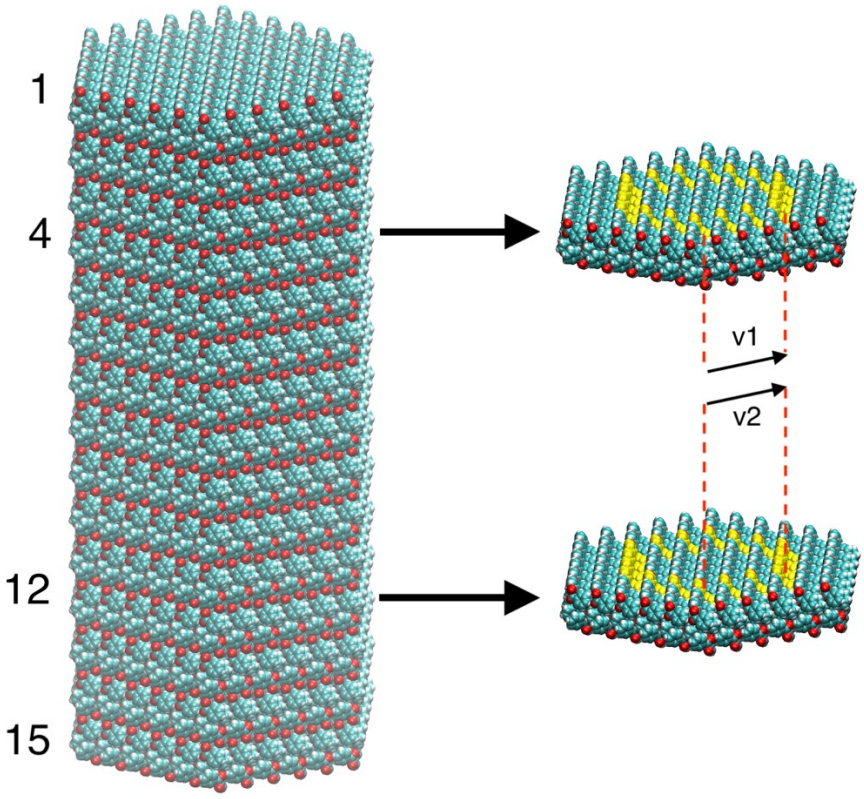

Figure S1. Scheme of calculation of twisting angles. Two layers on the right are extracted from the crystal positioned at ¼ and ¾ along *c*. Unit cells colored in yellow are used for calculating twisting angles, between matched vectors (otherwise translationally related) on two layers divided by the distance between the center of mass of two vectors along axial direction.

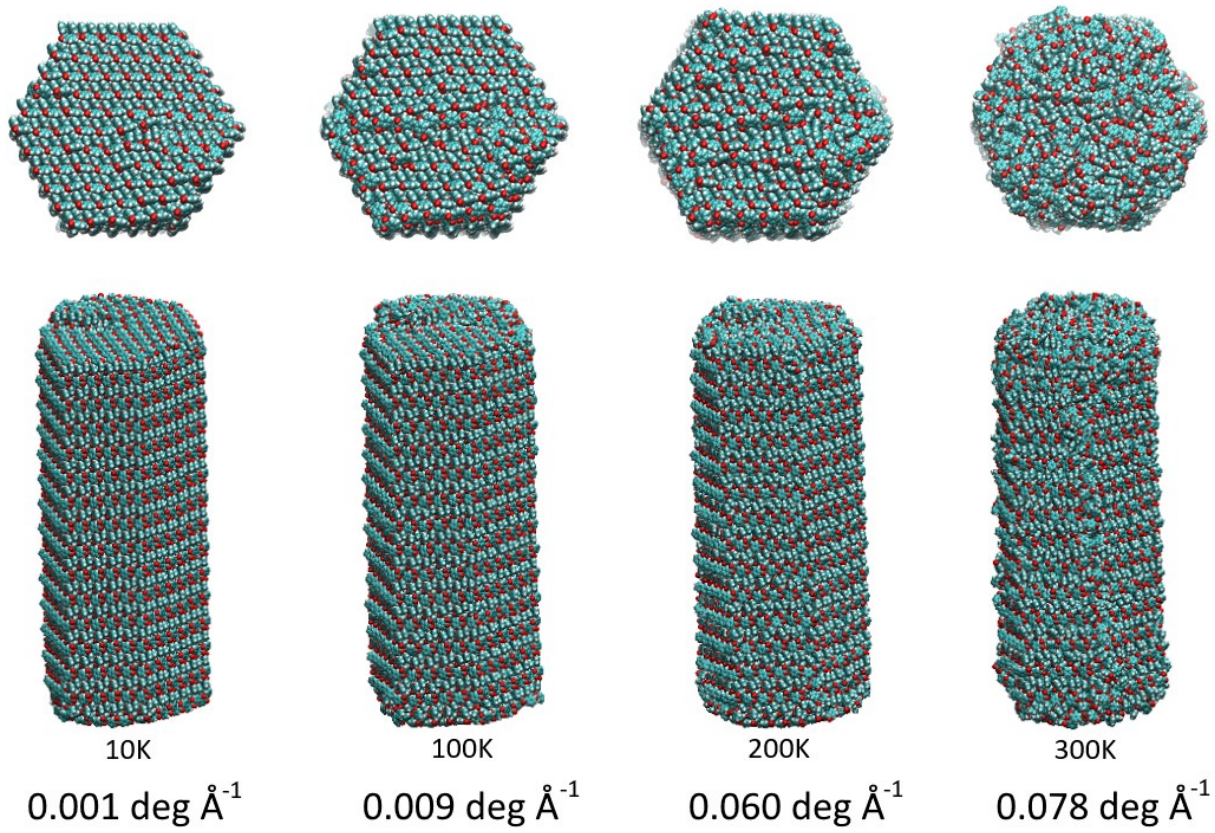

Figure S2. Representations of a $P3_221$ benzil nanocrystal rod (dimensions 6 x 6 x 15 unit cells) containing a right-handed dislocation obtained with molecular dynamics simulations at different temperatures, as viewed down the crystallographic c axis (upper row) and roughly perpendicular to the c axis (lower row). The corresponding Eshelby twisting angles (bottom) increase with increasing temperature. The twisting angle during the simulations at 10 K and 100 K did not change appreciably from the values observed just after the simulation was initiated, indicating that the twisting angle in each frame was near zero. Conversely, the twisting angles increase throughout the simulations at 200 K and 300 K, validating an Eshelby twist. At higher temperatures, the surface morphology became highly disordered, signifying melting and a reduction of crystalline order.

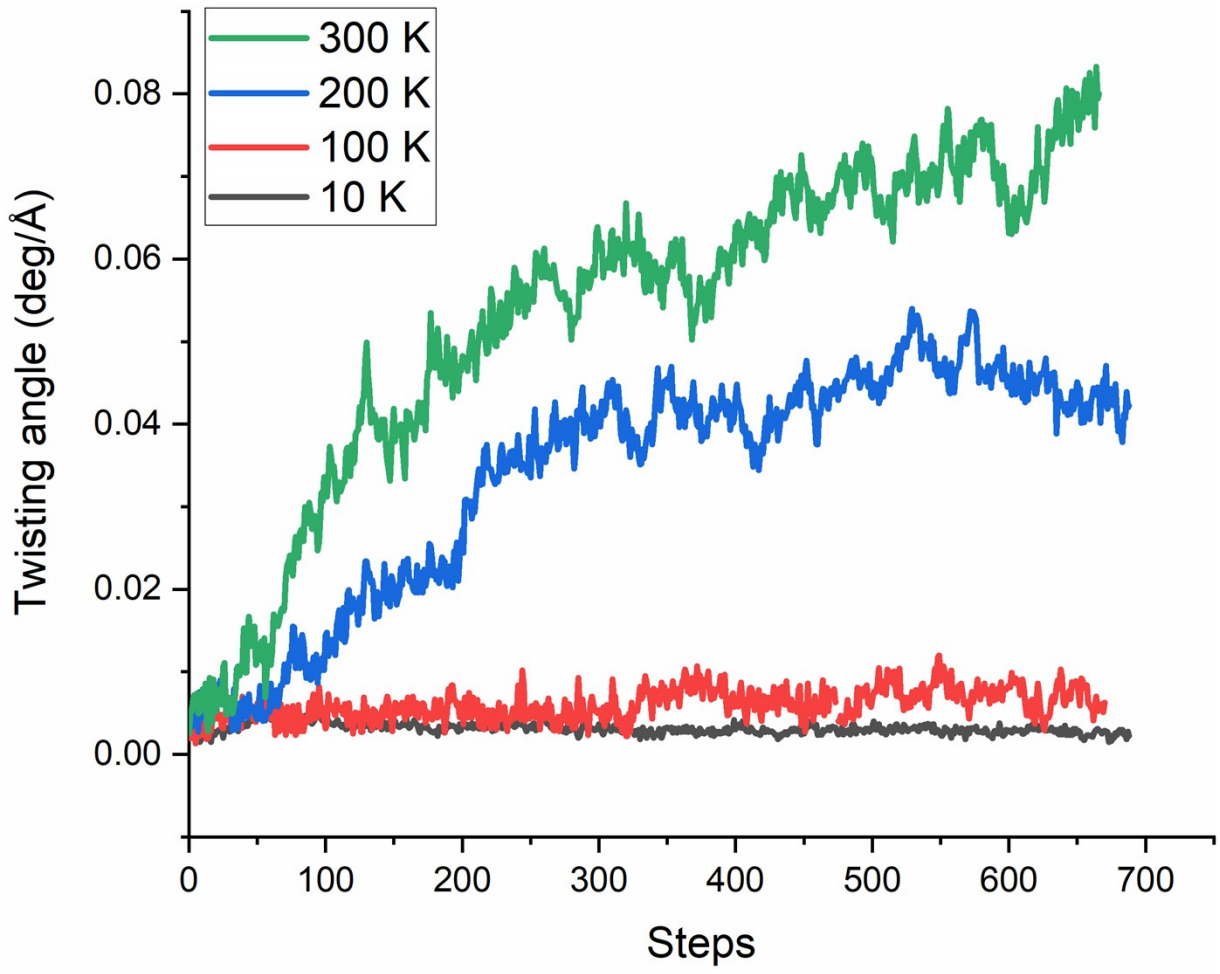

Figure S3. Twisting trajectories for $P3_221$ benzil nanorods ($6 \times 6 \times 15$ unit cells) with a right-handed dislocation, at different temperatures. At low temperatures (10 K and 100 K), twisting is negligible and unchanging throughout the simulation, consistent local minima that frustrate mechanical deformation.

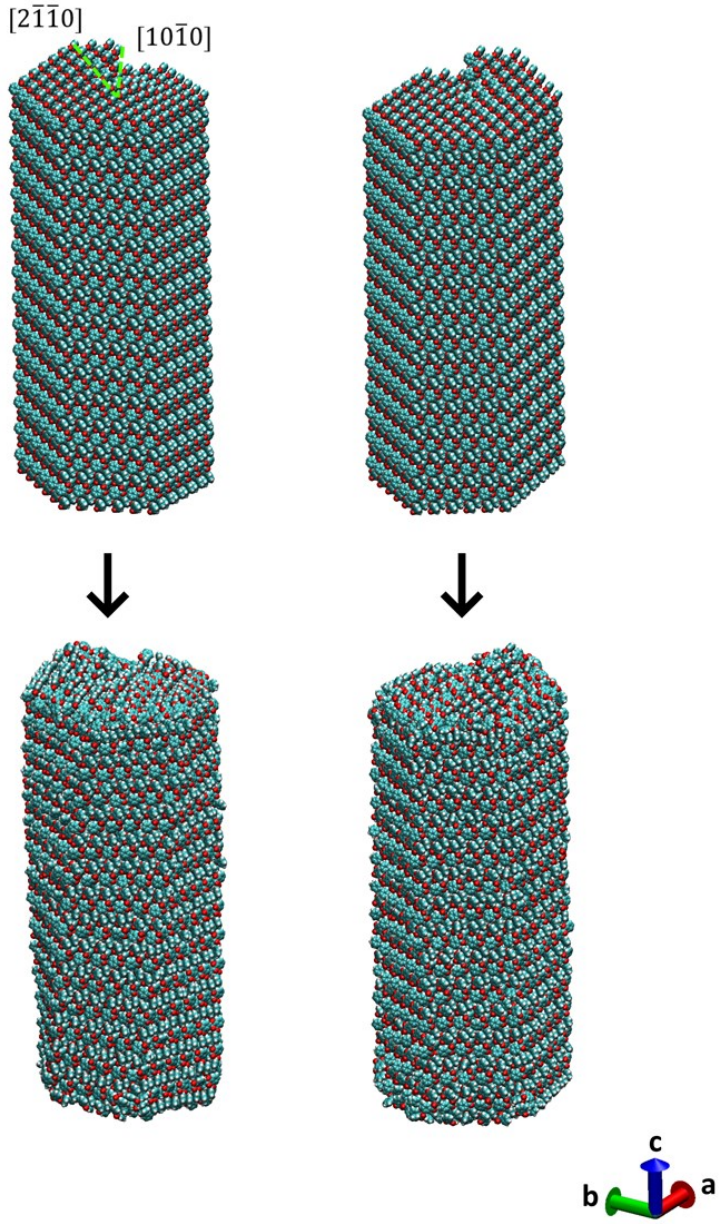

Figure S4. Twisting of $P3_221$ benzil nanocrystal rods (6 x 6 x 15 unit cells) with heterochiral shears in the $(1\bar{2}10)$ planes containing the $[10\bar{1}0]$ vector. The twisting angles for the rods with this dislocation are 0.22 deg Å^{-1} for the left-handed dislocation (left) and -0.060 deg Å^{-1} for the right-handed dislocation (right), both similar to the twisting angles of rods of same size and same space group sheared along the $[2\bar{1}\bar{1}0]$ direction on a $(01\bar{1}0)$ plane.

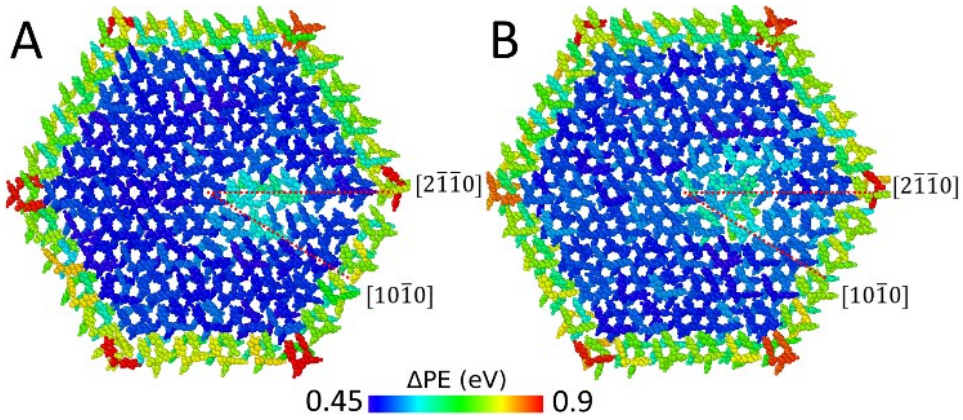

Figure S5. Potential energy of benzil nanorods of size 6×6×15, space group $P3_221$, viewed along *c*. Left-handed dislocation (A) and right-handed dislocation (B). Vectors in shear planes are indicated in red lines. Models shown correspond to shear containing horizontal [$2\bar{1}\bar{1}0$] vectors.

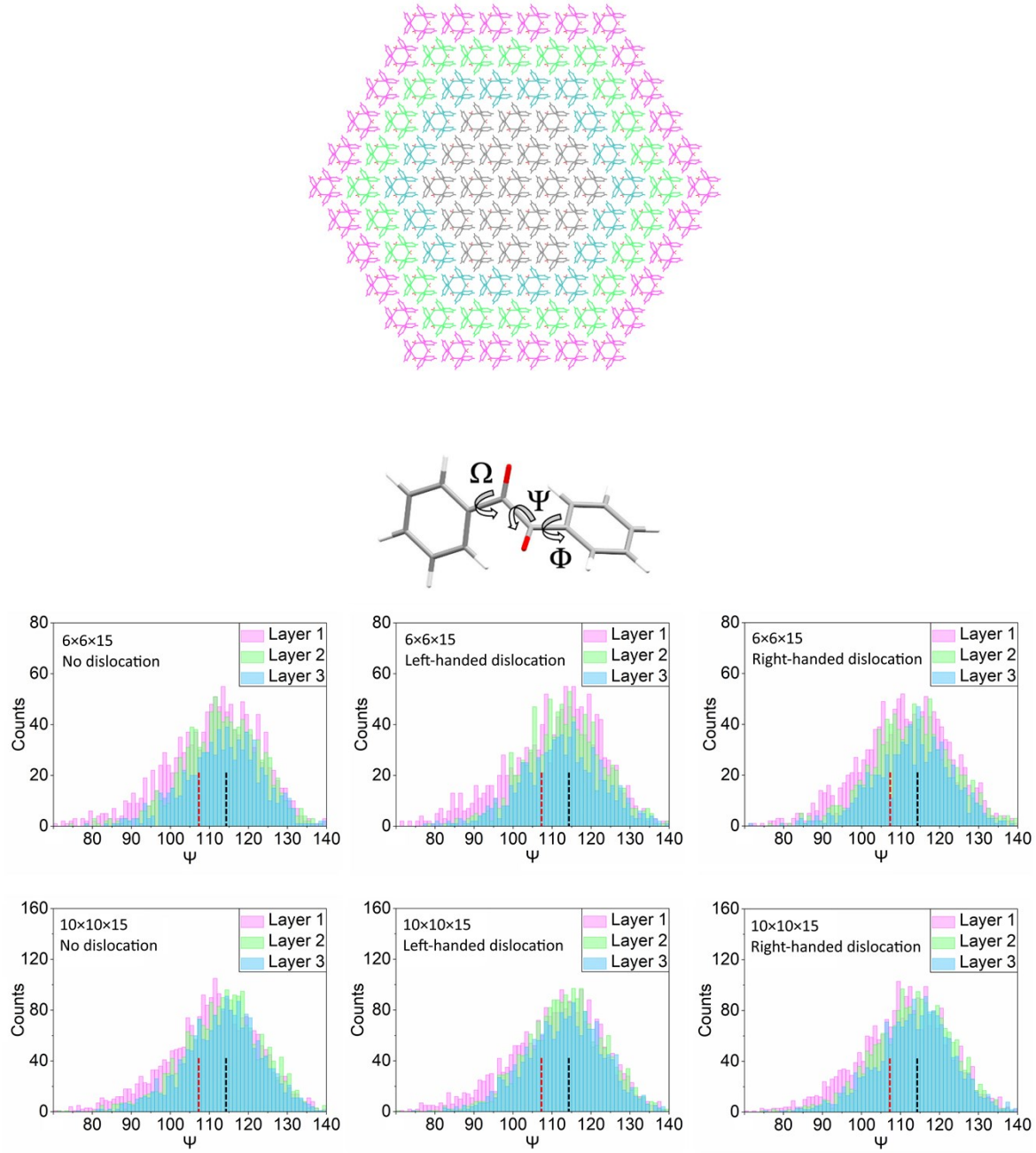

Figure S6. (top) Schematic representation of the three outermost layers of a benzil nanocrystal rod (6 x 6 x 15 unit cells), as viewed down the *c* axis. The layers are denoted by different colors that correspond to the legends in the histograms. (middle) Molecular structure of benzil, with the conformationally flexible angles denoted. (bottom) Histograms of the distribution of Ψ angle for benzil molecules in the first, second and third $(10\bar{1}0)$ layers (from outermost layer to inner layers) of 6 x 6 x 15 and 10 x 10 x 15 nanocrystal rods obtained from Molecular Dynamics simulations at 200 K. The histograms reveal that Ψ does not change with nanocrystal size in this regime and is independent of the presence and handedness of dislocations. Data for the Ψ angle only is presented here. The other two angles exhibit nearly identical statistical distributions.

References

1. J. Wang, R. M. Wolf, J. W. Caldwell, P. A. Kollman and D. A. Case, *J. Comput. Chem*., 2004, **25**, 1157−1174.
2. A. Nemkevich, H.-B. Bürgi, M. A. Spackman and B. Corry, *Phys. Chem. Chem. Phys*., 2010, **12**, 14916−14929.
3. S. Plimpton, *J. Comput. Phys*., 1995, **117**, 1−19.
4. E. Vanquelef, S. Simon, G. Marquant, E, Garcia, G. Klimerak, J. C. Delepine, P. Cieplak and F.-Y. Dupradeau, *Nucleic Acids Res*., 2011, **39**, W511−W517.
5. F. Wang, J. P. Becker, P. Cieplak and F. Y. Dupradeau, F. Y. R.E.D. Python: Object oriented programming for Amber force fields; Université de Picardie−Jules Verne, Sanford Burnham Prebys Medical Discovery Institute: 2013.
6. F. Y. Dupradeau, A. Pigache, T. Zaffran, C. Savineau, R, Lelong, N. Grivel, D. Lelong, W. Rosanski and P. Cieplak, *Phys. Chem. Chem. Phys*., 2010, **12**, 7821−7839.
7. C. I. Bayly, P. Cieplak, W. Cornell and P. A. A. Kollman, *J. Phys. Chem*., 1993, **97**, 10269−10280.
8. J. D. Gale and A. L. Rohl, *Mol. Simul*., 2003, **29**, 291-341.
9. J. D. Gale, *Z. Kristallogr. - Cryst. Mater*., 2005, **220**, 552-554.